Antimicrobial peptide-gold nanoscale therapeutic formulation with high skin regenerative potential

Michela Comune, Akhilesh Rai, Kiran K. Chereddy, Sandra Pinto, Sezin Aday, André F. Ferreira, Alessandra Zonari, Josephine Blersch, Rodrigo Cunha, Ricardo Rodrigues, Juan Lerma, Pedro N. Simões, Veronique Préat, Lino Ferreira

PII: S0168-3659(17)30705-8
DOI: doi: 10.1016/j.jconrel.2017.07.007
Reference: COREL 8862

To appear in: *Journal of Controlled Release*

Received date: 8 December 2016
Revised date: 1 July 2017
Accepted date: 6 July 2017

Please cite this article as: Michela Comune, Akhilesh Rai, Kiran K. Chereddy, Sandra Pinto, Sezin Aday, André F. Ferreira, Alessandra Zonari, Josephine Blersch, Rodrigo Cunha, Ricardo Rodrigues, Juan Lerma, Pedro N. Simões, Veronique Préat, Lino Ferreira , Antimicrobial peptide-gold nanoscale therapeutic formulation with high skin regenerative potential. The address for the corresponding author was captured as affiliation for all authors. Please check if appropriate. Corel(2017), doi: 10.1016/j.jconrel.2017.07.007

Antimicrobial peptide-gold nanoscale therapeutic formulation with high skin regenerative potential

Michela Comune[1], Akhilesh Rai[1,2], Kiran K. Chereddy[3], Sandra Pinto[1], Sezin Aday[1], André F. Ferreira[4], Alessandra Zonari[1], Josephine Blersch[1], Rodrigo Cunha[1], Ricardo Rodrigues[1], Juan Lerma[5], Pedro N. Simões[4], Veronique Préat[3], Lino Ferreira[1,2]

[1]CNC-Center for Neurosciences and Cell Biology, University of Coimbra, 3000, Coimbra, Portugal

[2]Faculty of Medicine, University of Coimbra, 3000-548, Coimbra, Portugal,
[3]Louvain Drug Research Institute, Pharmaceutics and Drug Delivery, Université Catholique de Louvain, Brussels, Belgium
[4]CIEPQPF, Department of Chemical Engineering, University of Coimbra, 3030-790 Coimbra, Portugal
[5]Instituto de Neurociencias, Centro mixto de la Universidad Miguel Hernández de Elche y el Consejo Superior de Investigaciones Científicas, 03550 San Juan de Alicante, Spain

ABSTRACT

Chronic skin wounds affect ≈3% of persons aged > 60 years[1]. These wounds are typically difficult to heal by conventional therapies and in many cases they get infected making even harder the regeneration process. The antimicrobial peptide (AMP) LL37 combines antimicrobial with pro-regenerative properties and thus represents a promising topical therapy to address both problems. Here, we investigated the wound healing potential of soluble and immobilized LL37 (LL37-conjugated gold nanoparticles, LL37-Au NPs), both *in vitro* (migration of keratinocytes) and *in vivo* (skin wound healing). Our results show that LL37-Au NPs, but not LL37 peptide, have the capacity to prolong the phosphorylation of EGFR and ERK1/2 and enhance the migratory properties of keratinocytes in a large *in vitro* wound model. We further report that both LL37 and LL37-Au NPs promote keratinocyte migration by the transactivation of EGFR, a process that seems to be initiated at the P2X7 receptor, as confirmed by chemical and genetic inhibition studies. Finally, we show *in vivo* that LL37-Au NPs have higher wound healing activity than LL37 peptide in a splinted mouse full thickness excisional model. Animal wounds treated by LL37-Au NPs have higher expression of collagen, IL6 and VEGF than the ones treated with LL37 peptide or NPs without LL37. Altogether, the conjugation of AMPs to NPs offers a promising platform to enhance their pro-regenerative properties.

Keywords: antimicrobial peptide, LL37, wound healing, purinergic receptors, P2X7 receptor, EGFR transactivation, keratinocytes

1. Introduction

Topical therapies that combine antimicrobial and pro-regenerative effects are of great potential in the context of skin wound healing. Antimicrobial peptides (AMPs) act as a first line of defense in the human body against bacteria, virus and fungi[2, 3], and some of them modulate regeneration processes[4]. In the last years, these small peptides (typically below 40 aminoacids) have been tested as a potential anti-infective therapy, at least for some indications, and thus an alternative to conventional antibiotics[5]. Currently, there are 10 AMP compounds in clinical trials, mostly for skin applications[5]. Two AMPs are in phase 3 clinical trials (to treat *C. difficile* infections and diabetic foot ulcers). Some of these AMPs combine antimicrobial properties (targeting microorganisms) with immunomodulatory, pro-angiogenic and tissue regenerative properties (both targeting human cells). For example, LL37 (one of the AMPs currently in clinical trials[6]) is an AMP predominantly found in human skin that acts at different levels of skin homeostasis[7]. LL37 is a chemoattractant of mast cells, monocytes, T lymphocytes and neutrophils, and regulates inflammation, angiogenesis and wound healing[4, 8]. The wound healing properties of LL37 peptide (either in a soluble formulation[4, 8, 9] or in a formulation consisting in polymeric nanoparticles releasing LL37[10]) has been demonstrated in wound animal models, as well as in a recent phase I/II clinical trial[6].

One of the approaches being tested to deliver AMPs *in vivo* and prevent their potential toxicity while increasing their stability against protease degradation and serum inactivation is through the chemical immobilization of AMPs in nanoparticles (NPs)[11-20]. We and others have recently demonstrated that AMP-conjugated NPs may offer higher stability, lower toxicity, enhanced antimicrobial properties (due to an increase in the local density of positive charges and peptide mass) and improved targeting compared with free AMP [11-13, 18, 19]. However, to the best of our knowledge, AMP-conjugated NPs have not been tested either *in vitro* or *in vivo* in the context of their regenerative potential relatively to soluble AMPs. It is unclear whether multivalent AMP-conjugated NPs may modulate cellular signaling and bioactivity. Although it has been demonstrated

that in some cases multivalent ligand-containing NPs have superior bioactivity than soluble ligands[21], such activity profile are likely dependent in the type of cellular target (e.g. receptor, protein, ionic channel) and type of cell.

Here, we investigated the wound healing potential of LL37-conjugated NPs both *in vitro* (migration of keratinocytes) and *in vivo* (skin wound healing). These NPs have a gold (Au) core and a hydrophilic cationic LL37 peptide shell. We have selected Au NPs because it is relatively easy the modification of their properties (e.g. size), the immobilization of high concentrations of AMPs per surface area[13], and they have a biomedical track[22]. LL37-conjugated NPs were prepared by a one step procedure[13]. Initially, the physico-chemical properties of LL37-Au NPs were characterized. To show the unique properties of LL37-Au NPs we have evaluated their pro-migratory properties against keratinocytes, an important player in the context of skin healing, and evaluated their mechanism relatively to LL37 peptide. Finally, we have evaluated *in vivo* the regenerative potential of LL37 and LL37-Au NPs in a splinted mouse full thickness excisional model. Overall our results indicate that LL37-conjugated NPs have enhanced wound-healing properties than LL37 peptide because they prolong in time the biological activity of the peptide.

2. Materials and methods

Detailed materials and methods section is provided in supplementary information.

2.1. Materials

$HAuCl_4.3H_2O$, $Na_3C_6H_5O_7$ and HEPES, all acquired to Sigma-Aldrich, were used as received. Lyophilized LL37 peptide modified with a C-terminal cysteine (LLGDFFRKSKEKIGKEFKRIVQRIKDFLRNLVPRTESC) was purchased from Caslo Laboratory, Denmark. The peptide was synthesized by conventional solid-phase synthesis, purified by high performance liquid chromatography, and characterized by matrix assisted laser desorption

ionization time-of-flight (MALDI-TOF) mass spectroscopy. The purity of the peptide was 96%. Rhodamine B isothiocyanate and HEPES were purchased from Sigma.

2.2. NP preparation

LL37 (0.5 mM) were dissolved initially in DMF (100 μL) followed by addition of HEPES (900 μL, 100 mM, pH 5). $HAuCl_4.3H_2O$ (10^{-2} M, 50 μL) was added to a peptide solution (0.25 mM, 950 mL; therefore the final concentration of $HAuCl_4$ was 0.5 mM) and the NP synthesis was carried out at 25 °C. LL37-Au NPs were also synthesized using $HAuCl_4.3H_2O$ (final concentration 0.25 mM, 0.5 mM and 1 mM), and HEPES (100 mM, pH 6 and pH 7.5) by the same procedure at 25 °C. The synthesized Au NPs were centrifuged at 14,000 rpm for 20 min at 4 °C followed by washing with Milli-Q water to remove unreacted peptides and HEPES, frozen and freeze-dried at 223 K using a Snijders Scientific freeze-dryer. Spherical Au NPs were also synthesized via citrate reduction method[23]. An aqueous $HAuCl_4$ solution (0.5 mM, 100 mL of water) was boiled in a 250 mL round bottom flask while being stirred after which an aqueous sodium citrate solution (2%, w/v, in water) was added. The reaction was allowed to run until the solution reached a wine red color, indicating the reaction was completed. Fluorescent Au NPs and LL37-Au NPs were prepared by addition of DMSO (0.5 mM) solution of rhodamine to achieve a final concentration of 25 μM for flow cytometry and confocal microscopy studies. Free rhodamine molecules in the colloidal gold solution were removed by centrifugation at 12,000 rpm for 15 min at 4 °C followed by one washings with Milli-Q water. The pellet obtained after centrifugation was redispersed in Milli-Q water and then dialysed. The methods for NP characterization are presented in the Supplementary Information.

2.3. Cell culture

Human keratinocyte cell line (HaCaT cell line, CLS, Eppelheim, Germany; passage 35-40)

and human primary keratinocytes (NHEK, PromoCell, Heidelberg, Germany; passage 3) were cultured as recommended by the vendor. Briefly, HaCaT cells were cultivated using DMEM supplemented with 1% (v/v) penicillin and streptomycin (Invitrogen) and 10% (v/v) fetal bovine serum (FBS, Invitrogen) until 90% of confluence. Human primary keratinocytes were cultured using KGM-2 media (PromoCell, Heidelberg, Germany). For cell passage, keratinocytes were initially trypsinized and then scraped. The cells were sub-cultured at a ratio of 1:3 until achieving the number of cells required for the experiment. The methods to evaluate the cytotoxicity, internalization and intracellular trafficking of LL37-Au NPs and LL37 peptide are described in detail in the supplementary information.

2.4. NP bioactivity

2.4.1 Scratch assay

Keratinocytes were seeded at a density of 2×10^4 cells/well in fibronectin-coated 96-well plate in DMEM supplemented with 1% (v/v) penicillin and streptomycin and 10% (v/v) FBS. After 48 h, cells were initially starved for 15 h in DMEM with 0.5% FBS, inactivated with mitomycin (5 μg/mL) for 2 h, and then incubated with LL37 (1 μg/mL), LL37- Au NPs or Au NPs (both at 200 μg/mL) for 5 h at 37 °C and 5% CO_2. In case of chemical inhibition, the chemical inhibitors for FPRL1 (WRW4, Calbiochem, 10 μM), EGFR (Erlotinib HCL, OSI-744, Selleck Chemicals, 2 nM), ADAM17 (Marimastat, Sigma, 10 μM), P2X (PPADS, Sigma, 100 μM), for P2X7 (A-740003, Sigma, at a concentration of 500 nM), were added to the cells 1 h before the incubation with LL37 peptide and LL37-Au NPs and then maintained during the assay. We tested all inhibitors used in our study, and none of them showed any significant toxicity to cells under our experimental conditions (data not shown). After the 5 h treatment, cells were washed twice with PBS to remove non-internalized NPs and a scratch was created with a sterile pipette tip. The detached cells were washed twice with PBS and then plates were re-coated with fibronectin (10 μg/mL in starvation

medium) for 1 h at 37 °C. Cells were washed and maintained in starvation medium up to 72 h. Cell migration was monitored overtime by a In Cell Microscope 2000 (GE Healthcare) (objective 2×). The cells treated with LL37 peptide were cultured with starvation medium containing LL37 for the entire duration of the experiment. Scratch areas were quantified using the AxioVision software (Carl Zeiss). Wound areas were normalized by the initial area (n= 6 images). In case of siRNA knock-down studies, on-target plus human ADAM17 siRNA or P2X7R siRNA (both from Dharmacon) were used to silence ADAM17 or P2X7 before performing the scratch assay. Keratinocytes were transfected with 50 nM siRNA using 0.25 µL of Lipofectamine RNAiMAX (Life Technologies) for 24 h in antibiotic-free complete medium before starting the scratch assay.

To test the prolonged effect of LL37-Au NPs on keratinocyte migration, cells were plated in fibronectin-coated 24-well plate (1×10^5 cells/well), after 48 h cells were starved for 15 h in DMEM with 0.5% FBS and then the scratch was made with a sterile pipette tip. Only after this step, the cells were incubated with LL37 (5 µg/mL), LL37-Au NPs and Au NPs (15 µg/mL) in starvation medium up to 96 h. During this time, cell migration was monitored by scratch area quantification. To test the effect of LL37-Au NPs in primary keratinocytes, cells were plated in a 24 well plate (pre-warmed for 1 h with 1 mL medium; cells added dropwise) (4×10^4 cells/well) and allowed to grow for 48 h until form a monolayer. After this, the cell layer was scratched using a sterile pipette tip and incubated in KGM-2 medium, without epidermal growth factor, supplemented with LL37-AuNP (15 µg/mL) or Au NPs (15 µg/mL) or soluble LL37 peptide (5 µg/mL) for 24 h. Cell migration was monitored using an automated microscope (In Cell 2000, GE Healthcare).

The methods for the quantification of EGFR and ERK1/2 phosphorylation are described in detail in the supplementary information.

2.4.2. Electrophysiological recordings

Whole-cell patch-clamp recordings of HaCaT cells were performed using borosilicate glass

patch pipettes with a resistance of 2-5 MΩ and compensating the series resistance by 50-60% with a List EPC-7 amplifier, as described previously[24]. The pipettes were filled with (in mM): 135 K-gluconate, 10 CsCl, 0.4 NaH_2PO_4, 0.73 $CaCl_2$, 1 $MgCl_2$, 1 EGTA, and 14 HEPES (pH 7.4). The external solution contained (mM): 140 NaCl, 3 KCl, 2 $CaCl_2$, 1 $MgCl_2$, 15 HEPES and 10 glucose (pH 7.4). Cells were rapidly perfused as previously described[25] and all experiments were carried out at RT (22-25 ºC). The currents were recorded at -70 mV, filtered (2-pole Butterworth filter, -12 dB/octave) and digitized to a personal computer at a sampling rate of 1 kHz for analysis using pCLAMP software (AXON instruments). Charge transfer was calculated by the integration of the area under the current in the first 100 s (Q100) from the beginning of the exposure to Au NPs, LL37 or LL37-Au NPs in the absence or presence of apyrase (darker background; 20 U/mL; Sigma).

2.5. In vivo wound healing and tissue collection

6–7 week old RjHan:NMRI female mice (Janvier, BE) were anesthesized with isoflurane and hair from dorsal area was shaved a day before the surgery. Two 0.5-mm-thick silicone (Grace biolabs, UK) donut-shaped splints (OD=20 mm, ID= 10 mm) were fixed on either side of the dorsal midline, approximately 3.5 cm from the ears and positioned with 6-0 nylon sutures (Monosof, USA). Full-thickness excisional wounds were made using an 8 mm round skin biopsy punch (Kai Europe GMBH, DE), centered within each splint. 10 mice were randomly assigned per group and were administered intradermally at several sites around the wound with only vehicle (0.9% w/v NaCl, Mini-Plasco, BE), LL37 (70 µg), LL37-Au NPs (200 µg) and Au NPs (200 µg) in autoclaved water by sterile insulin syringe (BD medical, France) as a dispersion in 30 µL of vehicle. Two wounds were made on each mouse to increase sample size and to avoid cross-contamination both wounds were administered with the same treatment. Thus, n=10 animals (20 wounds) per group. Wounds were covered with transparent sterile adhesive bandage (IV3000, Smith & Nephew, UK) followed by adhesive fabric tape (BSN medical, France) to prevent the chewing of splints by mice.

On days 0, 2, 5, 7, 10, 13 and 16 wounds were digitally photographed by Leica IC80 HD camera (Leica, Swiss). Optical zoom was maintained identical throughout the experiments. Wound areas were quantified using the Jmicro Vision software developed by N. Roduit at University of Geneva, Switzerland. Wound sizes are expressed as percentage of the initial respective wound. On day 5 and 10, three animals per group were sacrificed and wounds along with surrounding tissue were collected for further experiments and bisected into two halves. Remaining animals were sacrificed on day 16. The animal studies were approved by the animal care and ethical committee of health science sector, Université Catholique de Louvain. The methods for histology, immunhistochemistry, collagen quantification, MPO activity and gene analyses are provided in Supplementary Information.

2.6. Statistical analyses

Statistical analyses were performed by a t-test or one-way ANOVA test with a Newman-Keuls test applied post hoc for paired comparisons of means (GraphPad Prism 5.0 software).

3. Results

3.1. Synthesis and characterization of LL37-Au NPs

LL37 peptide modified with a cysteine at C-terminus was used to prepare in a single step LL37-conjugated Au NPs (**Fig. 1a**). Several reaction conditions, including initial concentration of Au ions (**Supplementary Fig. 1**), LL37 (**Supplementary Fig. 2**) and pH (**Supplementary Fig. 3**) were screened to obtain rapidly Au NPs with low size, relatively low polydispersity and high incorporation of LL37 (**Fig. 1a**). The first benchmarks were to obtain rapid LL37-Au NPs with diameters between 15 and 25 nm (Au NPs with diameters below 10 nm have higher toxicity against mammalian cells [26]), able to maintain their stability in aqueous solution. In the absence of HEPES buffer, no reduction of Au ions was observed by LL37 peptide (data not shown) while in

the absence of the LL37 peptide, Au NPs with high polydispersity were synthesized (**Supplemental Table 1**). Therefore, we screened several concentrations of Au ions and LL37 peptide in the presence of HEPES buffer at different pH values (5, 6 and 7.5). We selected HEPES buffer at pH 5 for the initial screening since at this pH the NPs were formed in a few hours (2-3 h) (**Fig. 1b**) in contrast to pH 6 or 7.5 (see below) which requires between 1 and 9 days, respectively (**Supplementary Fig. 3a**). In addition, LL37-Au NPs produced at pH 6.0 were largely non-spherical with large diameter (ca. 35 nm; **Supplementary Fig. 3e**) while the ones produced at pH 7.5 aggregated overtime (data not shown). Concentrations of Au ions of 0.5 mM and LL37 of 0.25 mM gave rise to NPs up to 1 day, with a relatively low polydispersity and a diameter of approximately 20 nm (**Supplementary Figs. 1 and 2**). Based on these results we selected for subsequent tests a Au ion concentration of 0.5 mM and LL37 of 0.25 mM to generate LL37-Au NPs in HEPES buffer at pH 5.0, as a compromise between NP synthesis rate, diameter, stability and polydispersity.

LL37-Au NPs had a SPR band centered at 530 nm (**Supplementary Fig. 3b**), a dominant spherical morphology (**Supplementary Fig. 3e**) and an average diameter of 21 ± 8 nm ($n \geq 100$) (**Supplementary Fig. 1c.1**), as determined by transmission electron microscopy (TEM) analyses. Fourier transformed infrared (FTIR) analyses indicated that LL37-Au NPs typically had a random coil structure (amide-I and amide-II bands at 1650 and 1582 cm^{-1}) as did LL37 peptide in aqueous solution (**Fig. 1c**). High-resolution thermogravimetric and zeta potential analyses showed that approximately 25% of the NP mass was organic (**Fig. 1d**) and the NPs were positively charged (+15.4 ± 2 mV), respectively. Quantification by spectrophotometry of LL37 peptides that were not conjugated to the Au NPs after reaction indicates that each Au NP had approximately 154 peptides conjugated.

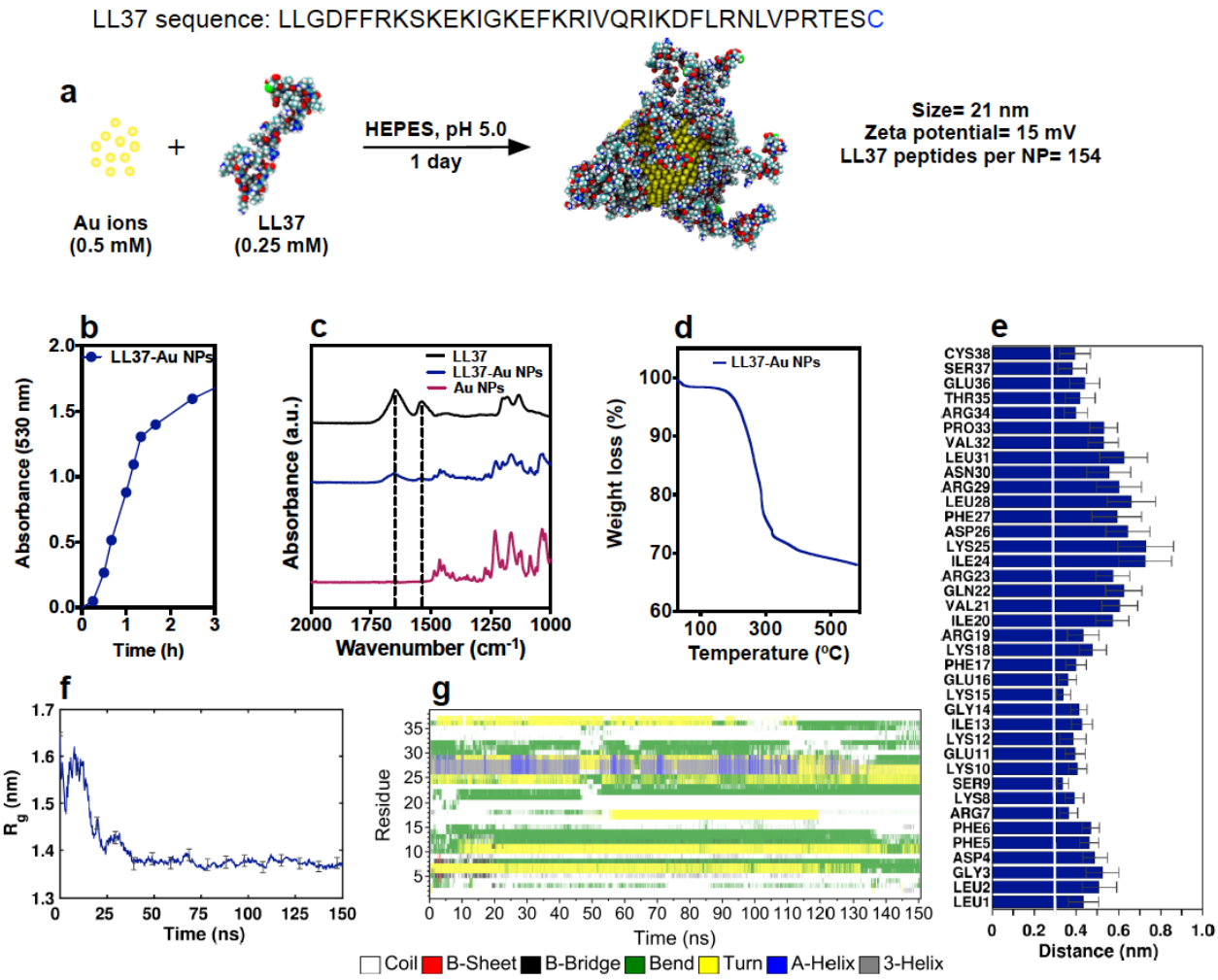

Figure 1 Synthesis and characterization of LL37-Au NPs. (a) Schematic representation of Au NP synthesis in the presence of LL37 peptide. (b) Time dependent absorbance for the synthesis of LL37-Au NPs in HEPES buffer pH 5.0 (Au ions=0.5 mM; LL37=0.25 mM). (c) FTIR and (d) TGA analyses of LL37 peptide, Au NPs and LL37-Au NPs. (e) Distance of LL37 aminoacid residues to the Au surface at the end of the simulation. Results are Average ± SEM, *n*=20. The line at 0.3 nm represents the cut-off used to define direct contact between the atoms of the amino acids and the Au surface. (f) Gyration radius profile of LL37 in LL37-Au NPs. Average ± SEM, *n*=20. (g) Time-course of LL37 peptide secondary structure in LL37-Au NPs. Aminoacid residues are identified by numbers that are displayed in figure e.

Molecular dynamic (MD) analyses showed that that most of the aminoacid residues took ca. 50 ns to achieve a stable position (**Supplementary Fig. 4**). The radius of gyration (*R*g) profile[27] suggests that the peptide conformation changes during the interaction with the Au NP, adopting a more compact structure after the immobilization process (**Fig. 1f**). At the end, some cationic residues of LL37 (ARG7, LYS8, LYS10, LYS12, LYS15, ARG19 and ARG34) as well as CYS38

(the terminal residue of LL37) were in contact (below 0.3 nm) with the surface of the NP while other cationic residues (LYS18, ARG23, LYS25 and ARG29) were distant (**Fig. 1e**). Although some regions of the peptide (the ones that are distant from the surface of the NP) seem to adopt an alpha-helix structure during the immobilization process, such structure is not present at the end of the simulation, suggesting that no clear secondary structure exists in the immobilized peptide (**Fig. 1g**).

To evaluate whether LL37-Au NPs maintained the bioactivity of LL37, we assessed their antimicrobial properties. The antimicrobial activity of the LL37-Au NPs (10 μg/mL, which corresponds to an immobilized concentration of 2.5 μg/mL of LL37) was evaluated against 10^5 CFU gram-negative (*E. coli*) bacteria in PBS buffer at 37ºC (**Supplementary Fig. 5**). Au NPs prepared in HEPES buffer without the LL37 peptide were used as a control. As expected, Au NPs had no antimicrobial activity. On the other hand, LL37-Au NPs or LL37 peptide (5 μg/mL) had high antimicrobial activity killing more than 75% of the microorganisms in 4 h. No antimicrobial activity was observed in the supernatant of the LL37-Au NPs, which indicated that the active peptide was not leached from the NP surface (data not shown).

3.2. LL37-Au NPs and LL37 interactions with keratinocytes

Human keratinocytes were chosen as a representative cell type with which the LL37-Au NPs may interact with in the skin. LL37-Au NPs were positively charged when resuspended in water; however, they became negatively charged after resuspension in keratinocyte culture medium (DMEM medium supplemented with 10% FBS) (**Supplementary Fig. 6a**). LL37-Au NPs did not sediment overtime but show some aggregation in cell culture media. To assess the biological effect of the NPs, cell viability was monitored by PI incorporation (**Supplementary Fig. 7a**), cell metabolism by ATP production (**Supplementary Fig. 7b**), cellular oxidative stress by the production of reactive oxygen species (ROS) (**Supplementary Fig. 7d**) and cell membrane impact

by cell depolarization studies (**Supplementary Fig. 7e**). LL37 and Au NPs have been used as controls. Keratinocytes treated with LL37 or LL37-Au NPs up to a concentration of 10 μg/mL and 400 μg/mL (ca. 100 μg/mL of LL37), respectively, have no significant decrease in cell viability or increase in ROS production. Yet, a decrease in cell viability and an increase in ROS production were observed for concentrations of LL37 equal or above 10 μg/mL. Keratinocytes became slightly hyperpolarized after 5 h exposure to LL37 peptide in solution at concentrations above 25 μg/mL, while the effect was lost at 48 h. Interestingly, the membrane potential of keratinocytes was depolarized after exposure to LL37-Au NPs or Au NPs for 48 h. These results suggest a likely interaction of NPs with cell membrane. Because our aim is to use LL37-Au NPs to treat chronic wounds we measured also its hemocompatibility. The LL37-Au NPs were determined to be relatively hemocompatible because they did not activate platelets aggregation (**Supplementary Fig. 7c**).

In some cases, the bioactivity of LL37 requires its cellular internalization[28-30]. Therefore we evaluated the internalization of LL37-Au NPs by inductively coupled plasma mass spectrometry (ICP-MS) (the internalization of LL37 peptide was evaluated below by confocal microscopy and flow cytometry). Human keratinocytes were able to uptake LL37-Au NPs (between 20 and 250 pg/cell depending in the initial concentration of NPs) although less effectively than Au NPs (having similar size; 2 to 7-fold lower, depending on the initial concentration and time of contact) as evaluated by ICP-MS (**Supplementary Fig. 8a**). The internalization of the NPs occurred essentially during the first 5 h since no significant increase was observed after 48 h of NP contact with the cells. To identify the mechanism of internalization of LL37 peptide and LL37-Au NPs, keratinocytes were incubated in the presence of endocytosis chemical inhibitors at concentrations that were not cytotoxic for the cells (**Supplementary Fig. 9a**), after which, rhodamine-labeled LL37-Au NPs or rhodamine-labeled LL37 were added and the internalization process monitored by flow cytometry (**Supplementary Fig. 8b.1**). Various inhibitors such as filipin III, nocodazole,

cytochalasin D, dynasore, polyinosinic acid/dextran sulfate and EIPA were used to inhibit cholesterol-dependent internalization, microtubule-dependent pathways, actin-dependent pathways, clathrin-mediated endocytosis, scavenger receptors and macropinocytosis pathways respectively [31, 32]. Whenever possible molecules that enter by a specific internalization pathway were used as positive controls to show the efficacy of our inhibitors (**Supplementary Fig. 9b**). The internalization of LL37-Au NPs and LL37 was mediated by endocytosis since significant inhibition was observed at 4ºC. Our results further show that LL37-Au NPs and LL37 were internalized mainly by scavenger receptors, since keratinocytes inhibited with polyinosinic acid or dextran sulfate had no significant NPs or LL37 peptide internalization (**Supplementary Figs. 8b.2 and 8b.3**). To confirm the endocytosis mechanisms involved in NP internalization, keratinocytes were transfected with siRNAs to down-regulate key components of different endocytic mechanisms (**Supplementary Figs. 8b.4 and 8b.5**). We observed a ~70% and 60% reduction on LL37-Au NPs and LL37 uptake, respectively, upon downregulation of class-A scavenger receptor 3 (SCARA3), confirming a role of scavenger receptors in NP internalization.

Next, we examined the intracellular trafficking of rhodamine-labeled LL37-Au NPs or rhodamine-labeled LL37 by confocal microscopy in keratinocytes. Images of cells reconstructed from z-stacks of confocal images indicated significant cellular uptake of NPs (**Fig. 2a and Supplementary Fig. 10**) and LL37 (**Supplementary Fig. 11**). Co-localization of LL37-Au NPs with EEA1 vesicles peaked at 4 h (ca. 25%) while co-localization with Rab7 peaked at 24 h (ca. 33%) (**Supplementary Fig. 9b**). Co-localization of LL37-Au NPs with EGFR during the 24 h was also observed. LL37 was also internalized by keratinocytes and 50% of LL37 was within EEA1 and Rab7 positive endolysosomal compartments up to 24 h (**Supplementary Fig. 11**). TEM results confirm that NPs are taken up by keratinocytes and localize within endolysosomal vesicles already after 30 min of NPs incubation (**Figs. 2b.1-2b.3**); however, foci of NPs interacting with the cell membrane are still visible at 4 h.

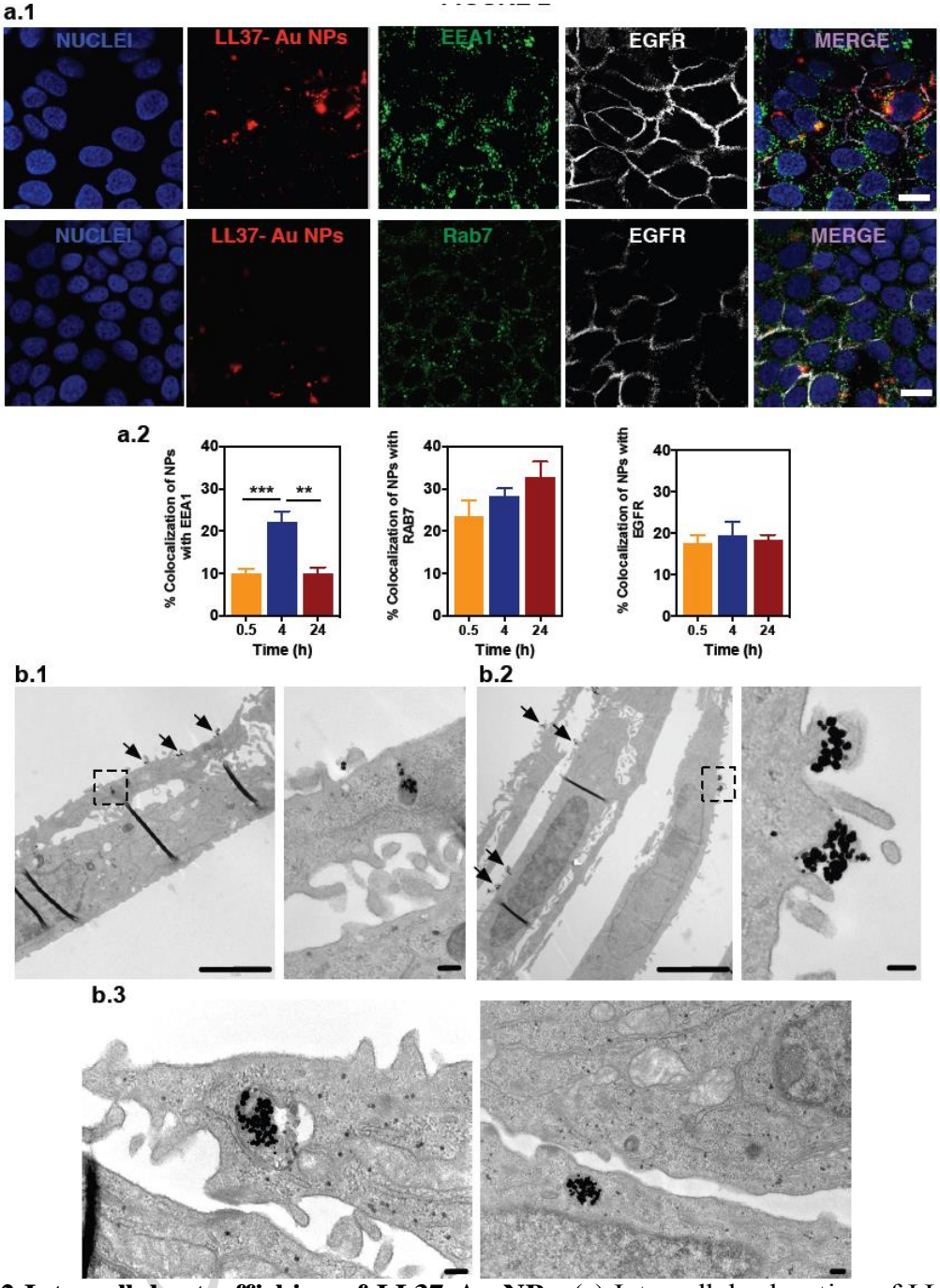

Figure 2 Intracellular trafficking of LL37-Au NPs. (a) Intracellular location of LL37-Au NPs in keratinocytes. (a.1) Keratinocytes were exposed to rhodamine-labeled LL37-Au NPs for 4 h. At the end, keratinocytes were washed and fixed before confocal microscopy characterization. Bar corresponds to 15 µm. (a.2) Quantification of the co-location of NPs with EEA1, Rab7 or EGFR. Results are Average ± SEM, from 6 different confocal images (40x objective). $^{**}P<0.01$ and $^{***}P<0.001$ indicates statistical significance between groups. (b) Characterization of LL37-Au NPs intracellular trafficking in keratinocytes by TEM. TEM results confirm that NPs are taken up by keratinocytes and localize within endolysosomal structures after 30 min (b.1), 4 h (b.2) and 24 h (b.3); however, some of the NPs are in contact with the cell membrane at least for 4 h. Arrows indicate sites of internalization. Cell spots defined by a dashed square means areas of magnification. In b.1 and b.2, bar corresponds to 2000 nm (left) and 100 nm (right, magnification). In b.3, bar corresponds to 100 nm.

Taken together, LL37-Au NPs and LL37 peptide are both internalized by keratinocytes mainly by scavenger receptors and a significant percentage (up to 50%) of both formulations accumulate in the EEA1 and Rab7-positive endolysosomal compartments. These results are in line with those obtained recently for macrophages that showed that LL37 accumulated in the endolysomal compartment[33]. However, both LL37-Au NPs and LL37 still co-localize with cell membrane (labeled by an epidermal growth factor receptor, EGFR, antibody) between 4 and 24 h post-exposure as shown by confocal microscopy (LL37 and LL37-Au NPs) and TEM (LL37-Au NPs).

3.3. Both LL37-Au NPs and LL37 peptide promote keratinocyte migration through P2X, ADAM17 and EGFR

Migration of keratinocytes is an important step in skin wound healing[9, 34]. Previous studies have shown that LL37 activates keratinocyte migration by the transactivation of EGFR[34] (**Fig. 3a**). This process involves the activation of metalloproteinases (likely ADAM10 and/or ADAM17) that releases EGF anchored to cell membrane into a heparin-binding EGF (HB-EGF), which in turn binds to EGFR[35]. This leads to the phosphorylation of ERK1/2 [36] and STAT3, translocation of STAT3 into the nucleus and finally the initiation of the transcription of target genes. So far little is known about how this cascade is initiated. Therefore, we have studied the pro-migratory properties of LL37 peptide, LL37-Au NPs and Au NPs by an *in vitro* scratch assay in keratinocytes for 72 h (**Fig. 3b**). Initially, the expression of putative receptors of LL37 in keratinocytes was evaluated by flow cytometry. Keratinocytes expressed high levels of EGFR, FPRL-1, a receptor that has been described to mediate the bioactivity of LL37 in endothelial cells [4], and P2X7, a receptor that has been described to mediate the bioactivity of LL37 in fibroblasts[37] and monocytes[38] (**Supplementary Fig. 12**). Next, we evaluated whether the migration of keratinocytes was due to the transactivation of EGFR. Both LL37 peptide and LL37-

Au NPs induced the migration of keratinocytes. The inhibition of FPRL-1 by the antagonist WRW4 [39] had no measurable effect in the migration of keratinocytes; however, the inhibition of EGFR by Erlotinib decreased significantly the migration of keratinocytes treated with LL37 peptide or LL37-Au NPs (**Figs. 3c.1 and 3c.2**).

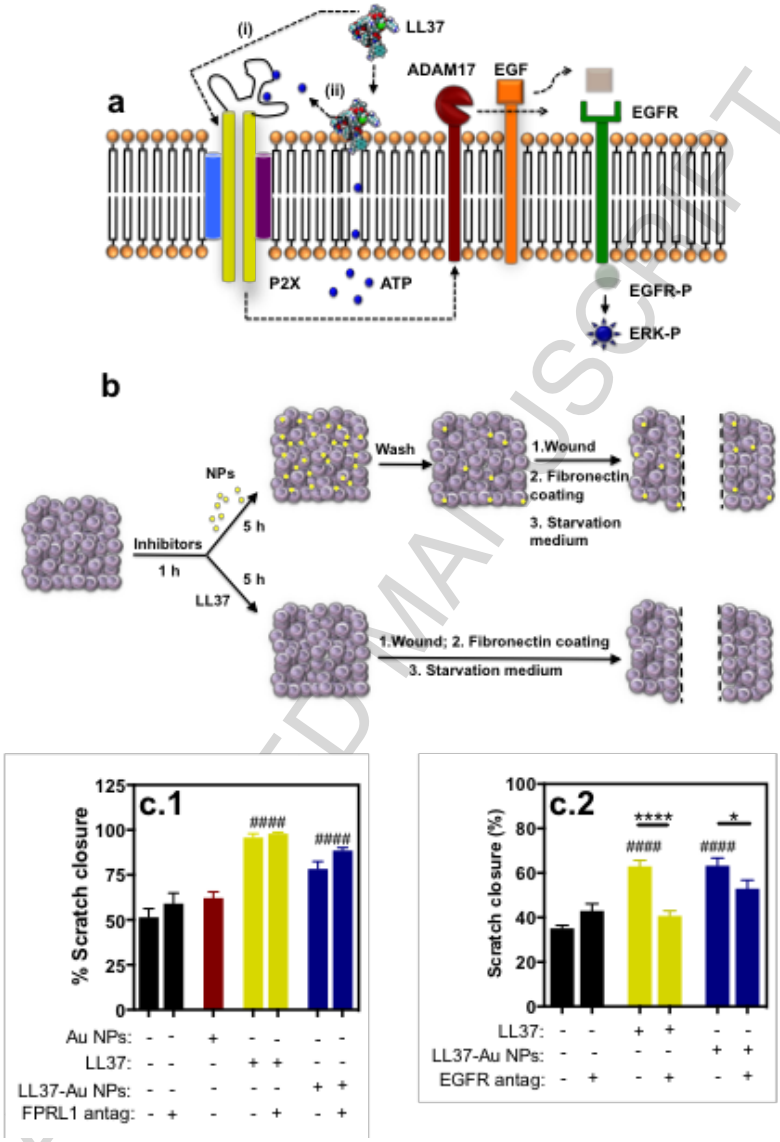

Figure 3 Bioactivity of LL37-Au NPs: scratch assay. (a) Schematic representation of the transactivation mechanism of EGFR. (b) Scratch assay. Confluent keratinocytes were starved for 15 h in DMEM with 0.5% FBS and then incubated for 1 h with specific inhibitors followed by the incubation for 5 h with LL37, LL37-Au NPs or Au NPs. Cells were then washed with PBS, a scratch was created, the plates re-coated with fibronectin, cells were again washed and maintained in starvation medium up to 72 h. Cell migration was monitored by a high-content microscope. (c) Scratch closure at 48 h post-treatment. Final wound area was normalized by initial wound area. Results are average ± SEM, n=6. The following chemical inhibitors have been used: WRW4 as a FPRL1 receptor inhibitor and Erlotinib as EGFR receptor inhibitor. $^{\#}P<0.05$, $^{\#\#}P<0.01$, $^{\#\#\#}P<0.001$ and $^{\#\#\#\#}P<0.0001$ indicates statistical significance relatively to control (cells without treatment).

*P<0.05, **P<0.01, ***P<0.001 and ****P<0.0001 indicates statistical significance between treatment groups.

To show the involvement of metalloproteases in the transactivation of EGFR we have performed the scratch assay in the presence of Marimastat, a general ADAM inhibitor (**Fig. 4a.1**). The pro-migratory properties of both LL37 and LL37-Au NPs significantly decreased in the presence of the ADAM inhibitor. Because studies have shown the involvement of ADAM17 in the transactivation of EGFR[36] we performed knockdown studies for ADAM17 using siRNA (**Fig. 4a.2**). Our results clearly show that the inhibition of ADAM17 decreased the migratory properties of keratinocytes after activation by LL37 or LL37-Au NPs.

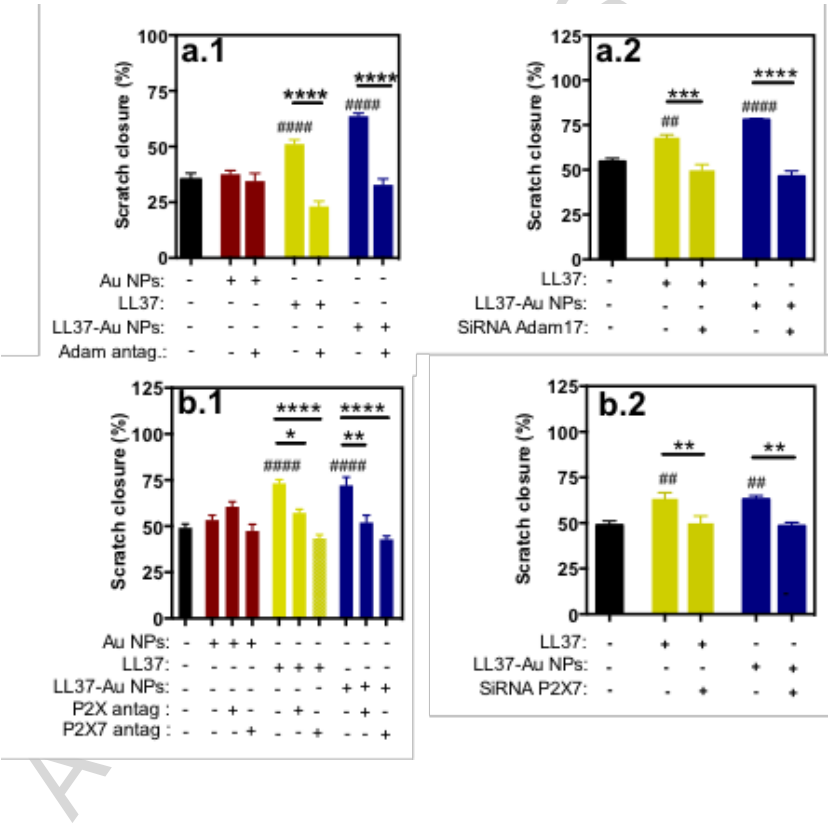

Figure 4 Bioactivity of LL37-Au NPs: scratch assay. Scratch closure (at 48 h post-treatment) in keratinocytes treated with inhibitors of metalloproteases (a) and P2X receptors (b) and then exposed to LL37, LL37-Au NPs or Au NPs. Final wound area was normalized by initial wound area. Results are average ± SEM, n=6. The following chemical inhibitors have been used: Marimastat an ADAM metalloprotease inhibitor, PPADS a generic P2X receptor antagonist and A-740003 a selective P2X7 receptor antagonist. $^{\#}P$<0.05, $^{\#\#}P$<0.01, $^{\#\#\#}P$<0.001 and $^{\#\#\#\#}P$<0.0001 indicates statistical significance relatively to control (cells without treatment). *P<0.05, **P<0.01, ***P<0.001 and ****P<0.0001 indicates statistical significance between treatment groups.

Recent studies have suggested that LL37 binds non-specifically to purinergic (P2X) receptors on the basis of their cationic[40] or hydrophobic[33] properties; however, no experimental evidence has been reported so far. To show the involvement of purinergic receptors in the transactivation of EGFR we have performed the scratch assay in the presence of pyridoxalphosphate-6-azophenyl-2',4'-disulfonic acid tetrasodium salt (PPADS)[37, 41], a broad-spectrum purinergic receptor antagonist (**Fig. 4b.1**). Our results show that keratinocyte migration was inhibited after activation with LL37 or LL37-Au NPs. In addition, PPADS treatment decreased significantly the phosphorylation of ERK1/2 a downstream target of EGFR transactivation (**Supplementary Fig. 13**). Because it has been hypothesized recently that LL37 binds non-specifically to P2X7 receptors[33, 40], we inhibited chemically the receptor by A-740003[42, 43] (**Fig. 4b.1**) or siRNA (**Fig. 4b.2**). In both cases, keratinocyte migration was inhibited after activation with LL37 or LL37-Au NPs. Moreover, immunocytochemistry analyses show co-localization of LL37-Au NPs or LL37 with P2X7 (**Fig. 5**).

To further confirm the involvement of P2X receptors in the LL37-Au NPs and LL37 activity in keratinocytes we performed electrophysiological recordings. In whole-cell patch-clamped keratinocytes at a holding potential of -70 mV, the exposure to either LL37 peptide, LL37-Au NPs or Au NPs elicited an inward current (**Fig. 6a**). We next attempted to evaluate if the observed inward currents were mediated by ATP-gated P2X channels. For that purpose, we evaluated the impact of apyrase, an enzyme that converts ATP into AMP, to the inward-currents elicited by the different compounds. We observed that the presence of apyrase reduced the charge transfer (Q) triggered by Au NPs and LL37-Au NPs but not by LL37. Whole-cell patch-clamp recordings showed that LL37-Au NPs (**Fig. 6a.3**) or Au NPs (**Fig. 6a.1**) triggered the release of extracellular ATP from keratinocytes, which in turn activated P2X receptors. If cells were treated with apyrase after the pulse with LL37-Au NPs or Au NPs there was a significant decrease in the inward electric current. In contrast, whole-cell patch-clamp recordings showed that LL37 peptide (**Fig. 6a.2**) did

not trigger the release of extracellular ATP because no decrease in the inward electric current was observed after treatment with apyrase (**Figs. 6a.2 and 6b).**

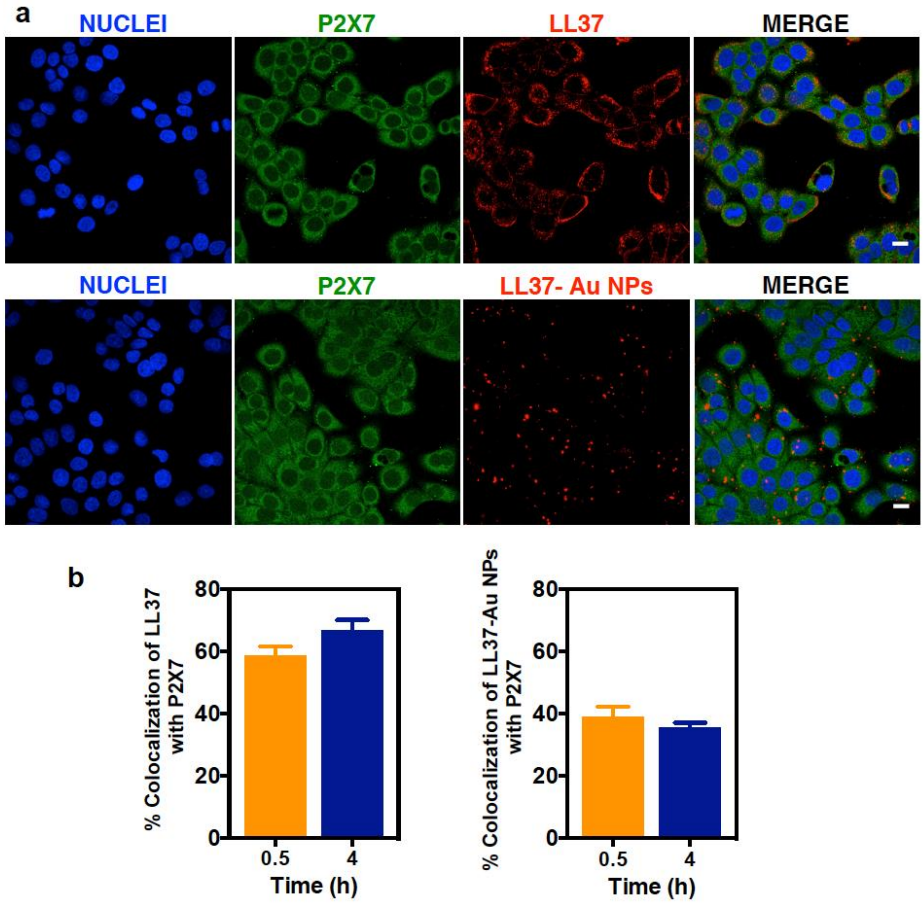

Figure 5 Co-localization studies between soluble LL37 and LL37-AuNPs with P2X7 in HaCaT cells. (A) Representative confocal images showing the co-localization between LL37 or LL37-AuNPs with P2X7. Cells were exposed for 30 min to LL37-Au NPs or LL37. Bars correspond to 15 µm. (b) Quantification of the co-localization. Analyses were performed according to the protocol described in Supplementary Information. Results are Average ± SEM, n=3 (3 independent runs; 4 image analyses for each run).

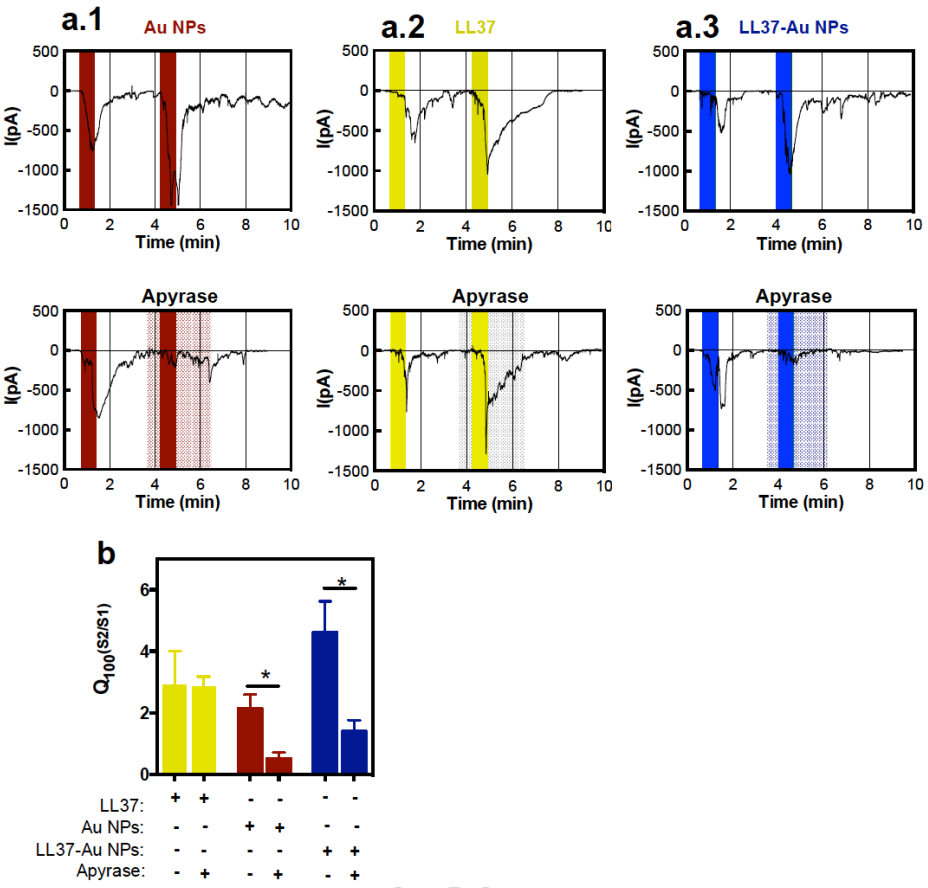

Figure 6 Bioactivity of LL37-Au NPs: electrophysiology studies. (a) Representative traces of inward-currents recorded in whole cell patch-clamped HaCaT cells at a holding potential of -70 mV exposed to (a1) Au NPs, (a.2) LL37 or (a.3) LL37-Au NPs. Forty single cells were exposed twice to the different treatments and the inward currents recorded presented a reproducible ratio between the charge transfer measured in the first 100 s (Q_{100}) in the second exposure (S2) over the first exposure (S1) as quantified in (b). The inward currents triggered by Au NPs and LL37-Au NPs, but not by LL37 were attenuated by the presence of apyrase, as observed by a reduced charge transfer in S2 in the presence of apyrase (darker background), as depicted in the lower traces in (a) and quantified by a reduced S2/S1 ratio shown in (b). Data are presented as mean ± SEM of the ratio of Q_{100} in S2 over S1 measured from 4-5 different cells per condition. **P*<0.05 unpaired *t*-test.

Overall, our results indicate that LL37 peptide and LL37-Au NPs promote keratinocyte migration by the transactivation of EGFR. The process in both cases is likely initiated at the P2X7 receptors, as confirmed by chemical and genetic inhibition studies. The activation of P2X receptors by LL37-Au NPs, but not by LL37 peptide, involves the release of extracellular ATP.

3.4. LL37-Au NPs prolong EGFR and ERK phosporylation and keratinocyte migration

compared to LL37 peptide

Epithelial wounding induces activation of EGFR and its two major downstream effectors PI3K and extracellular signal-regulated kinase ERK[44]. We have evaluated the phosphorylation of EGFR in keratinocytes mediated by LL37 peptide and LL37-Au NPs. In line with previous results[34], the phosphorylation of EGFR by LL37 peptide was rapid (peaked at 8 min) and persisted for 10 min (**Fig. 7a.1**). Interestingly, the phosphorylation of EGFR by LL37-Au NPs peaked at 10 min of contact and persisted for at least 60 min. The phosphorylation level was not significantly affected using a lower concentration of LL37-Au NPs (15 μg/mL). In addition, LL37-Au NPs lose their capacity to prolong the phosphorylation of EGFR in keratinocytes if washed after 10 min of contact, indicating that EGFR phosphorylation is dependent on NP-cell contact time (**Fig. 7a.2**).

Next, we examined whether the prolonged phosphorylation of EGFR was correlated with a prolonged phosphorylation of ERK1/2 [36]. The phosphorylation of ERK1/2 in keratinocytes by LL37 peptide peaked at 4 min and then decreased at time 30 min, while the phosphorylation of ERK1/2 in cells by LL37-Au NPs peaked at 30 min (**Fig. 7b**). Thus, our results confirm a correlation between EGFR and ERK1/2 phosphorylation.

To evaluate the functional impact of the prolonged phosphorylation of EGFR we have conducted a scratch assay in which the wound was large enough to evaluate the long-term migratory activity of keratinocytes (human HaCaT cell line and human primary keratinocytes). Keratinocytes treated with LL37-Au NPs had significantly higher migratory capacity than cells activated with LL37 or the other controls (**Figs. 7c and 7d**).

Taken together, our results show that LL37-Au NPs but not LL37 peptide have the capacity to prolong the phosphorylation of EGFR and ERK1/2 (from few minutes up to 1 h) and thus enhancing the migratory properties of keratinocytes in a large *in vitro* wound model.

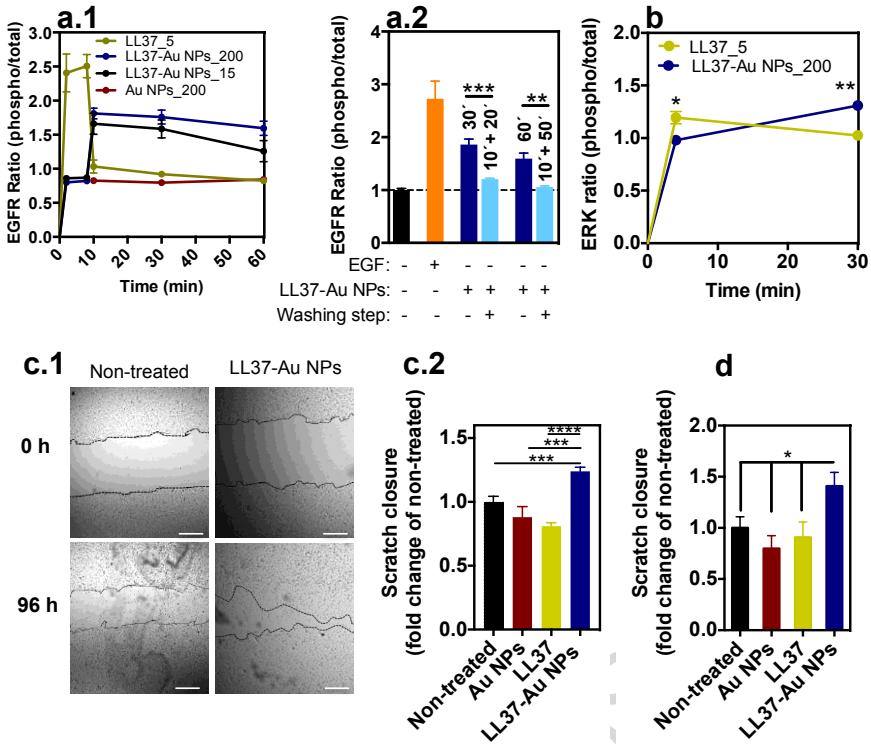

Figure 7 Bioactivity of LL37-Au NPs: molecular studies. (a.1) Phosphorylation profile (phospho/total protein) of EGFR in keratinocytes after contact with LL37 (5 µg/mL), LL37-Au NPs (15 or 200 µg/mL) or Au NPs (200 µg/mL) for a certain time (up to 60 min). (a.2) Phosphorylation profile of EGFR in keratinocytes after contact with LL37-Au NPs (200 µg/mL) with or without washing the LL37-Au NPs. The "10´+ 20´" on top of the column means that cells were washed after 10 min of contact with LL37-Au NPs and then cultured for more 20 min in medium without NPs. Epidermal growth factor (EGF) has been used as positive control. Results are average ± SEM, *n*=3. (b) Phosphorylation profile (phospho/total protein) of ERK without washing the LL37-Au NPs in contact with keratinocytes. Results are average ± SEM, *n*=3. (c) Scratch assay of keratinocytes (HaCaT cells) after 96 h of incubation with LL37 peptide (5 µg/mL), Au NPs (15 µg/mL) and LL37-Au NPs (15 µg/mL). (c.1) Light microscopy images of the healing of the scratch at 96 h. Bars correspond to 1 mm. (c.2) Quantification of scratch closure at 96 h. Results are average ± SEM, *n*=3-8. (d) Scratch closure in human primary keratinocytes at 24 h. Results are average ± SEM, *n*=5-8. In graphs a, b c and d, **P*<0.05, ***P*<0.01, *** *P*<0.001 and **** *P*<0.0001 indicate statistical significance between treatment groups.

3.5. LL37-Au NPs have higher *in vivo* wound healing activity than LL37 peptide

To further verify the biological effects of LL37-Au NPs wound healing experiments were performed in a splinted mouse full thickness excisional acute wound model. The freshly created wounds were immediately treated with LL37 peptide, LL37-Au NPs, Au NPs or non-treated (control). The concentrations of LL37 and LL37-Au NPs were chosen to be equivalent in terms of

LL37 concentration, based in TGA analyses performed for each NP batch. Wound area was monitored over a period of 10 days. At day 5, LL37-Au NP-treated mice showed an acceleration of wound healing as compared to the control (**Fig. 8a and Supplementary Fig. 14**). LL37-Au NP-treated mice showed complete wound healing after 10 days, whereas LL37 peptide-treated mice showed 70% healing after 10 days. No adverse effects on body weight, general health, or behavior of the mice was observed after NP treatment. The effect of LL37-Au NPs on wound healing was assessed by histological and immunohistochemical examination of epithelial gap closure. Skin sections were stained with hematoxylin and eosin (H&E) for general observation of skin layers and the extent of collagen deposition in healed tissue was determined by Masson's Trichrome (MT) staining. On day 5, the thick scab and the epithelium layer were formed in wounds treated with LL37-Au NPs compared to LL37 and Au NP-treated wounds (**Fig. 8e**). In addition, the wounds treated with LL37-Au NPs have higher levels of collagen than the ones treated with LL37 and Au NP-treated wounds, as shown by Sircol quantification (**Fig. 8b**). At day 10, a prominent thick epithelium layer was developed in LL37-Au NPs group and wound re-epithelization and deposition of connective tissue processes were mostly completed, leading to closure of wound (**Fig. 8e**).

It has been shown that IL6 is involved in wound healing by regulating leukocyte infiltration, angiogenesis, collagen accumulation and LL37-mediated keratinocyte migration [45, 46]. Epidermal keratinocytes have been identified as the main source of IL6 production in the skin and several host defense peptides including LL37 have been shown to stimulate IL6 expression [47, 48]. Therefore, we evaluated the expression of IL6 in the wounds of all the experimental groups by qRT-PCR. Wounds treated with LL37-Au NPs had higher expression of IL6 than wounds treated with LL37 or Au NPs (**Fig. 8c**). We extended these studies to quantify neutrophil infiltration in wounds by myeloperoxidase (MPO) analysis. MPO is an enzyme that is found predominantly in the azurophilic granules of neutrophils and can be used as a quantitative index of inflammatory infiltration[49]. MPO activity in wound tissue was significantly decreased after treatment with

LL37 peptide and LL37-Au NPs on day 10, demonstrating anti-inflammatory properties of LL37 peptide **(Fig. 8d)**. No reduction in MPO activity was found in wound tissue treated with Au NPs.

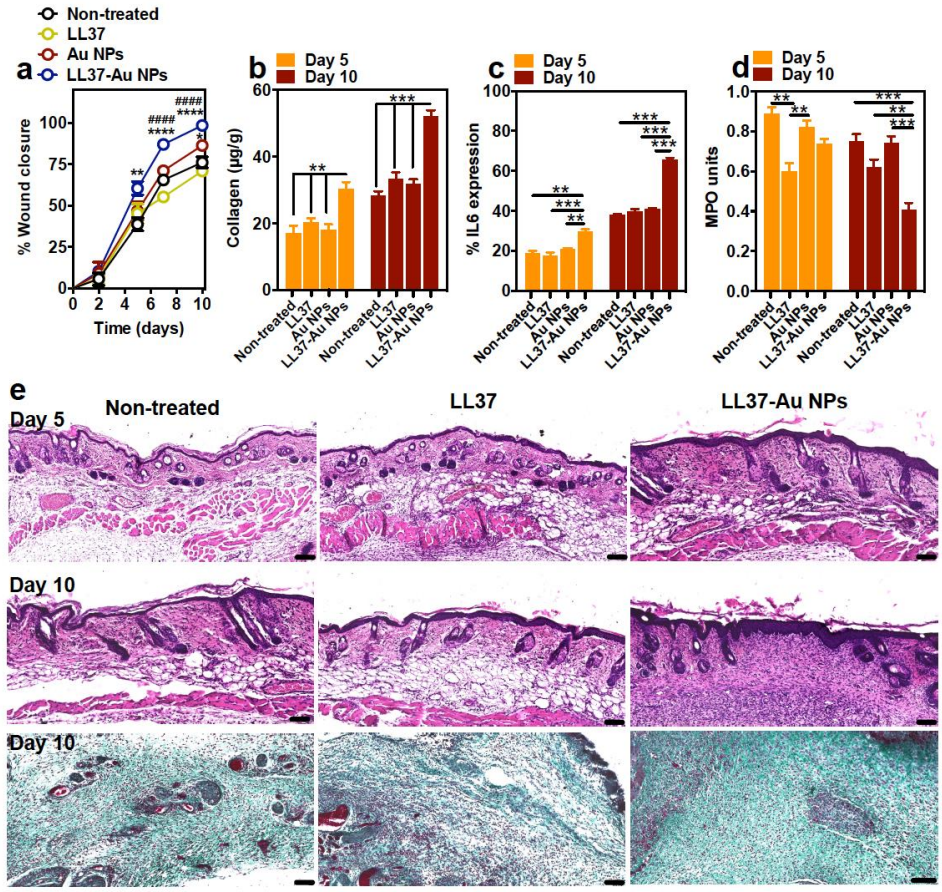

Figure 8 ***In vivo*** **wound healing properties of LL37-Au NPs: granulation tissue and inflammation.** (a) Wound closure in wounds treated with vehicle, LL37 peptide, Au NPs or LL37-Au NPs. The formulations were administered intradermally at several sites around the wound. Ten animals (therefore 20 wounds) were used per each group. Results are average ± SEM, n=20. (b) Quantification of collagen at days 5 and 10 by a Sircol assay. Results are average ± SEM, n=10. (c) Quantification of IL6 by qRT-PCR at days 5 and 10. Results are average ± SEM, n=10. (d) Quantification of myeloperoxidase (MPO) activity at days 5 and 10. Results are average ± SEM, n=10. (e) Histological analysis (Hematoxylin & Eosin staining and Masson trichrome staining) of wound tissues at day 5 and 10 of treatment. In graphs a, b, c and d, *P<0.05, **P<0.01, ***P<0.001 and ****P<0.0001 indicates statistical significance between treatment groups. In graph **a**, statistical significance is against non-treated animals (labeled with *) and against LL37 (labeled with #).

Next, the impact of LL37 and LL37-Au NPs in the vascularization of the wounds was assessed. The levels of VEGF were quantified by qRT-PCR and expressed as percentage relatively to control **(Fig. 9a).** Our results show that wounds treated with LL37-Au NPs have higher

expression of VEGF at day 10 than wounds treated with LL37 or Au NPs. Similarly, wounds treated with LL37-Au NPs have higher levels of CD31 than wounds treated with LL37 or Au NPs at day 10 (**Fig. 9b**).

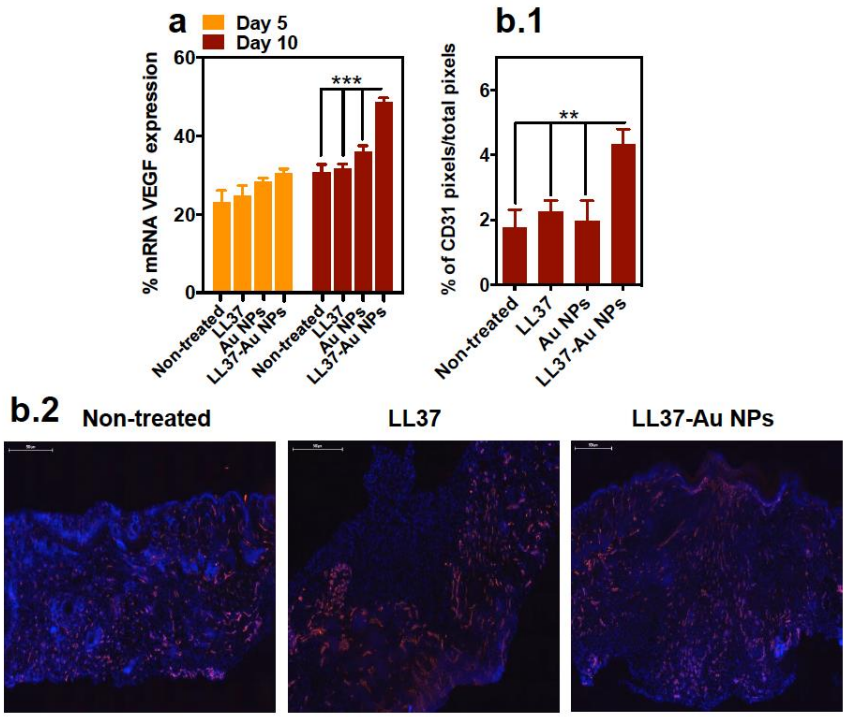

Figure 9 ***In vivo*** **wound healing properties of LL37-Au NPs: neovascularization.** Wounds were treated with vehicle, LL37 peptide, Au NPs or LL37-Au NPs. (a) qRT-PCR VEGF expression in wounds at day 5 and 10. Results are average ± SEM, n=10. (b.1) Quantification of CD31 staining. The percentage of red pixel represents both endothelial and red blood cells. Results are expressed as percentage of red pixels over the total amount of pixels within the analyzed surface. Results are average ± SEM, n=10. (b.2) Representative immunofluorescent images. Cells were labeled with DAPI and an antibody against CD31 (red). Bars correspond to 500 µm. $^{**}P<0.01$ and $^{***}P<0.001$ indicates statistical significance between treatment groups.

The interactions between skin and colloidal Au NPs of different physicochemical characteristics have been previously investigated [50, 51]. We decided to investigate the accumulation of LL37-Au NPs in the skin after topical administration and in the main organs of the mouse full thickness excisional model. LL37-Au NPs accumulated in the skin, being 74% of the initial concentration of the NPs found in the skin at day 2; however, only 10% of the initial concentration of NPs was found at day 15 (**Fig. 10a**). Less than 1% of the topical dose was found in the main organs at days 2 and 15. The toxic effects of the LL37-Au NPs against liver

(transaminase-GPT), kidney (urea), lung and general damage (lactate dehydrogenase) were also measured after 48 h of exposure (**Fig. 10b**). The topical administration of the LL37-Au NPs did not elevate the levels of these key parameters, indicating that the NPs did not cause significant damage to organ functions at the tested doses.

Overall, our results show that LL37-Au NPs have higher wound healing activity than LL37 peptide in an acute wound model. Our results further show that LL37-Au NPs are eliminated from the skin.

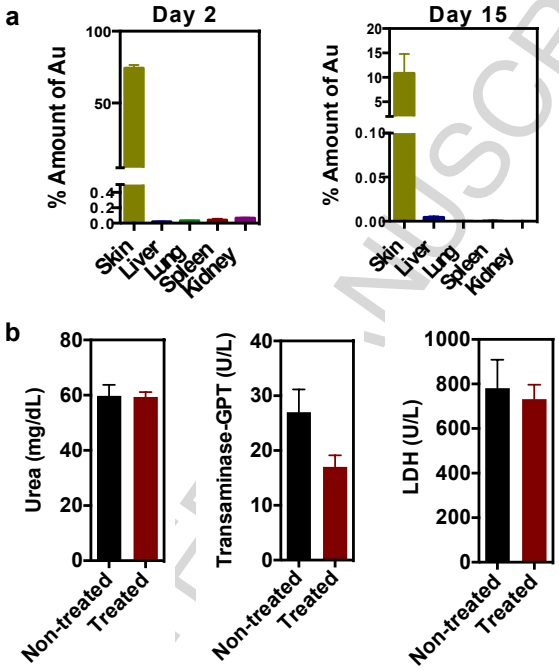

Figure 10 *In vivo* distribution of LL37-Au NPs. (a) Au content in different organs of mice at day 2 and 15, as quantified by ICP-MS. Animals were injected with a single dose (1 mg per animal) of LL37-Au NPs. Results are average ± SEM, *n*=5. **(b)** *In vivo* evaluation of biochemical parameters after 2 days exposure to LL37 Au NPs. Blood serum collected at day 2 was analyzed for the following biochemical parameters: urea, transaminase-GPT and LDH. No relevant changes between NP-treated and non-treated animals were observed.

4. Discussion

Here we show that the delivery mode of LL37 has an important effect in its biological activity. Our results show that LL37 conjugated to Au NPs have higher *in vitro* (pro-migratory properties against keratinocytes) and *in vivo* (skin wound healing) bioactivity than soluble LL37.

Our results further indicate that LL37-Au NPs activate P2X7 receptor followed by a prolonged transactivation of EGFR and enhanced migratory properties of keratinocytes in a *in vitro* wound model.

Several nanomedicine-based therapies have been reported in the last few years for wound healing[51, 52]; however, very few formulations combined antimicrobial with pro-regenerative properties. This is very important since many chronic wounds get infected during healing and thus the combination of both properties in the same therapeutic formulation is very beneficial[53]. Conventional NP delivery systems release their cargo by diffusion or following the degradation of the carrier. The delivery of the bioactive agent chemically immobilized to the NP is a route not often explored. Recent studies have shown that NPs coated with ligands/biomolecules, including siRNA [51], might have enhanced biological function than the corresponding soluble ligand counterpart [13, 21]. The density of the ligands/biomolecules as well as the nanoparticle size influences the bioactivity of the molecule. The binding and activation of membrane receptors might depend in the ligand multivalency and controlled spacing of the multivalent ligands[21, 54]. Our functional data suggests that LL37 peptide and LL37-Au NPs activate keratinotyces by P2X7 receptors followed by the activation of ADAM17 and the transactivation of EGFR. Keratinocytes inhibited by general purinergic receptor antagonists or by specific P2X7 receptor inhibitors (chemical or genetic) have decreased migration after activation by LL37 peptide or LL37-Au NPs. Our electrophysiology results suggest that the activation of P2X receptors by LL37 does not involve extracellular ATP. Indeed recent experimental results in mononuclear cells suggest that the biological role of LL37 is likely mediated by a complex between LL37 and P2X7R [33]. P2X7R forms a large multimolecular complex with several proteins in the plasma membrane such as β-actin, integrin β2, heat shock proteins and non-muscle myosin [33]. Moreover, the direct or indirect (by one of the co-associated molecules) activation of P2X7R can trigger PLD, MAPK- or PI3K-mediated downstream signaling pathways [55]. From our results and data in the literature is still

unclear whether there is a specific domain(s) of P2X7R or some co-associated adhesion molecule that mediates the binding of LL37. Importantly, in case of LL37-Au NPs, the activation of P2X receptors seems to be mediated in part by extracellular ATP. Cell treatment with apyrase decreased significantly, but not all, the inward electric current. Because Au NPs also induce the release of extracellular ATP but have no significant effect in the migratory properties of keratinocytes it is likely that the activation mechanism of LL37-Au NPs might involve other mechanisms than extracellular ATP. Therefore, we speculate that the activation of P2X receptors by LL37-Au NPs is due to a combinatorial effect by extracellular ATP and the direct/indirect interaction of LL37 of the surface of the NP with P2X7R.

To the best of our knowledge, this is the first study documenting the long-lasting phosphorylation of keratinocytes activated through purinergic receptors. The prolongation of EGFR phosphorylation may be explained by (i) an increased recycling rate of EGFR or (ii) retention of the phosphorylated EGFR at the plasma membrane preventing EGFR desphosphorylation[56]. Prolongation of EGFR phosphorylation has been described in some studies associated with the prevention of EGFR desphosphorylation. For example, the association of EGFR with the receptor erbB2, a major interaction partner and coactivator of EGFR, is sufficient to prolong and enhance the net phosphorylation of EGFR [57]. CTEN, a focal adhesion molecule of tensin family, is also able to extend the life of phosphorylated EGFR by decreasing EGFR reduction though the decrease of EGFR ubiquitination [58]. Moreover, EGF immobilized in two-dimensional surfaces is able to prolong the phosphorylation of EGFR [59]. Our results suggest that the prolongation of EGFR phosphorylation by LL37-Au NPs might be mediated by the retention of the phosphorylated EGFR at the plasma membrane preventing EGFR desphosphorylation. We observed co-localization of LL37-Au NPs with P2X7 and EGFR up to 4 h of contact by confocal microscopy analyses and we observed interaction of the NPs with the cell membrane until the 4 h of contact by TEM analyses. However, our experimental results cannot rule out the possibility that the prolongation of EGFR

may also be mediated during NP internalization.

LL37-Au NPs have higher wound healing activity than LL37 peptide in an acute wound model. The wound healing mechanism of LL37-Au NPs is mediated by an increased IL6 production, decreased inflammation (as evaluated by myeloperoxidase activity) and increased neovascularization. Although our work is the first study to demonstrate the *in vivo* wound healing properties of immobilized LL37, the *in vivo* wound healing properties of LL37 peptide have been previously demonstrated in animal models [4, 8, 9] and in phase I/II clinical trials [6]. The primary safety and tolerability end-point for LL37 was met for patients with venous leg ulcers. The results showed that patients treated with LL37 (twice per week; 0.5 mg/mL) had a statistically significant improved healing rate compared with placebo. However, the peptide was administered twice per week and thus LL37-Au NPs may offer an alternative approach to extend the bioactivity of the peptide in a single administration. Recently, we have reported a delivery system of LL37 based on the encapsulation of the peptide in poly(lactic-*co*-glycolic acid) nanoparticles [10]. It has been shown that the sustained release of LL37 could accelerate wound healing; yet the regenerative profile was more discrete than the one observed in this study. It is possible that the superior wound healing properties of LL37-Au NPs to LL37 might involve different cells of the skin and not only keratinocytes. For example, LL37 has important immunomodulatory effects that were not studied in this work[29, 30, 60, 61]. Depending in the environment and cellular context, LL37 may present pro-inflammatory or anti-inflammatory properties[60]. It has been shown that LL37 regulates the differentiation of monocytes in pro-inflammatory macrophages[29]. However, the anti-inflammatory properties of LL37 have been also demonstrated in various cell types[60].

The formulation reported here has an Au core and a hydrophilic cationic peptide shell, and makes use of an innovative one-step synthetic scheme recently reported by us [13]. In this synthetic scheme, the peptide acts as a capping agent and affects the kinetics of Au NP formation, likely due to the complexation of the peptide with the Au ions [13]. We have selected Au NPs because it was

relatively easy to control their size while presenting a high density of LL37 in their surface and because of their history in the context of wound healing [51, 62]. Interestingly, the LL37-Au NPs have different physico-chemical properties than cecropin-mellitin conjugated Au NPs (CM-Au NPs) previously described by us [13]. LL37-Au NPs are efficiently synthesized at pH 5 and aggregate at pH 7 while CM-Au NPs are efficiently synthesized at pH 7.5. In addition, the size of NPs (LL37-Au NPs: ≈25 nm; CM-Au NPs: ≈14 nm) and the number of peptide per NP (LL37-Au NPs: ≈150 nm; CM-Au NPs: ≈240 nm) are different in LL37-Au NPs and CM-Au NPs, when similar initial concentrations of peptide and gold ions were used. The differences found are likely explained by the size and sequence of the peptides.

Our *in vivo* biodistribution studies showed that most of the NPs (90%) are eliminated from the skin at day 15 post-application (therefore 5 days after wound closure) and residual (less than 0.05%) amount of NPs are found in the major organs. Although further tests are needed to evaluate the *in vivo* accumulation of NPs our results suggest that most of the NPs are eliminated from the skin.

5. Conclusions

Here we report an AMP-nanoscale therapeutic formulation with high skin regenerative potential, obtained in a rapid one-step synthetic process. LL37-Au NPs have higher *in vitro* (keratinocyte migration assay) and *in vivo* (skin wound healing assay) bioactivity than soluble LL37 peptide. The enhanced activity of LL37-Au NPs relatively to LL37 peptide is due to a prolonged activation of EGFR in keratinocytes, likely due to the retention of the phosphorylated EGFR at the plasma membrane preventing EGFR desphosphorylation. The results presented here are an exciting first step toward the development of AMP-based nanotherapeutics for skin disorders paving the way for additional studies in more complex animal models.

Acknowledgements. The authors would like to thank the financial support of EC (ERC project nº 307384, "Nanotrigger"; Marie Curie ITN "NANODRUG", FP7-PEOPLE-2011-ITN). The work was also funded by COMPETE in the context of the project "Stem cell based platforms for Regenerative and Therapeutic Medicine" (Centro-07-ST24-FEDER-002008).

References

1. Davies, C.E., et al., *A prospective study of the microbiology of chronic venous leg ulcers to reevaluate the clinical predictive value of tissue biopsies and swabs*. Wound Repair Regen, 2007. **15**(1): p. 17-22.

2. Zasloff, M., *Antimicrobial peptides of multicellular organisms*. Nature, 2002. **415**(6870): p. 389-95.

3. Hancock, R.E. and H.G. Sahl, *Antimicrobial and host-defense peptides as new anti-infective therapeutic strategies*. Nat Biotechnol, 2006. **24**(12): p. 1551-7.

4. Koczulla, R., et al., *An angiogenic role for the human peptide antibiotic LL-37/hCAP-18*. J Clin Invest, 2003. **111**(11): p. 1665-72.

5. Fox, J.L., *Antimicrobial peptides stage a comeback*. Nat Biotechnol, 2013. **31**(5): p. 379-82.

6. Gronberg, A., et al., *Treatment with LL-37 is safe and effective in enhancing healing of hard-to-heal venous leg ulcers: a randomized, placebo-controlled clinical trial*. Wound Repair Regen, 2014. **22**(5): p. 613-21.

7. Vandamme, D., et al., *A comprehensive summary of LL-37, the factotum human cathelicidin peptide*. Cell Immunol, 2012. **280**(1): p. 22-35.

8. Ramos, R., et al., *Wound healing activity of the human antimicrobial peptide LL37*. Peptides, 2011. **32**(7): p. 1469-76.

9. Carretero, M., et al., *In vitro and in vivo wound healing-promoting activities of human cathelicidin LL-37*. J Invest Dermatol, 2008. **128**(1): p. 223-36.

10. Chereddy, K.K., et al., *PLGA nanoparticles loaded with host defense peptide LL37 promote wound healing*. J Control Release, 2014. **194**: p. 138-47.

11. Maleki, H., et al., *High Antimicrobial Activity and Low Human Cell Cytotoxicity of Core-Shell Magnetic Nanoparticles Functionalized with an Antimicrobial Peptide*. ACS Appl Mater Interfaces, 2016. **8**(18): p. 11366-78.

12. Rai, A., et al., *High-density antimicrobial peptide coating with broad activity and low cytotoxicity against human cells*. Acta Biomater, 2016. **33**: p. 64-77.

13. Rai, A., et al., *One-step synthesis of high-density peptide-conjugated gold nanoparticles with antimicrobial efficacy in a systemic infection model*. Biomaterials, 2016. **85**: p. 99-110.

14. Bi, L., et al., *Designing carbohydrate nanoparticles for prolonged efficacy of antimicrobial peptide*. Journal of Controlled Release, 2011. **150**(2): p. 150-156.

15. Chen, W.Y., et al., *Self‐Assembly of Antimicrobial Peptides on Gold Nanodots: Against Multidrug‐Resistant Bacteria and Wound‐Healing Application*. Advanced Functional Materials, 2015. **25**(46): p. 7189-7199.

16. Eby, D.M., K.E. Farrington, and G.R. Johnson, *Synthesis of bioinorganic antimicrobial peptide nanoparticles with potential therapeutic properties*. Biomacromolecules, 2008. **9**(9): p. 2487-2494.

17. Mei, L., et al., *Bioconjugated nanoparticles for attachment and penetration into pathogenic bacteria*. Biomaterials, 2013. **34**(38): p. 10328-10337.

18. Liu, L.H., et al., *Self-assembled cationic peptide nanoparticles as an efficient antimicrobial agent*. Nature Nanotechnology, 2009. **4**(7): p. 457-463.

19. Wang, H., et al., *The efficacy of self-assembled cationic antimicrobial peptide nanoparticles against Cryptococcus neoformans for the treatment of meningitis*. Biomaterials, 2010. **31**(10): p. 2874-81.

20. Vignoni, M., et al., *LL37 peptide@silver nanoparticles: combining the best of the two worlds for skin infection control*. Nanoscale, 2014. **6**(11): p. 5725-8.

21. Jiang, W., et al., *Nanoparticle-mediated cellular response is size-dependent*. Nat Nanotechnol, 2008. **3**(3): p. 145-50.

22. Thakor, A.S., et al., *Gold nanoparticles: a revival in precious metal administration to patients*. Nano Lett, 2011. **11**(10): p. 4029-36.

23. Turkevich, J., P.C. Stevenson, and J. Hillier, *A Study of the Nucleation and Growth Processes in the Synthesis of Colloidal Gold*. Discussions of the Faraday Society, 1951(11): p. 55-&.

24. Marques, J.M., et al., *CRMP2 tethers kainate receptor activity to cytoskeleton dynamics during neuronal maturation*. J Neurosci, 2013. **33**(46): p. 18298-310.

25. Paternain, A.V., et al., *A role for extracellular Na+ in the channel gating of native and recombinant kainate receptors*. J Neurosci, 2003. **23**(25): p. 8641-8.

26. Yen, H.J., S.H. Hsu, and C.L. Tsai, *Cytotoxicity and immunological response of gold and silver nanoparticles of different sizes*. Small, 2009. **5**(13): p. 1553-61.

27. Lobanov, M., N.S. Bogatyreva, and O.V. Galzitskaia, *[Radius of gyration is indicator of compactness of protein structure]*. Mol Biol (Mosk), 2008. **42**(4): p. 701-6.

28. Lau, Y.E., et al., *Interaction and cellular localization of the human host defense peptide LL-37 with lung epithelial cells*. Infect Immun, 2005. **73**(1): p. 583-91.

29. van der Does, A.M., et al., *LL-37 directs macrophage differentiation toward macrophages with a proinflammatory signature*. J Immunol, 2010. **185**(3): p. 1442-9.

30. Bandholtz, L., et al., *Antimicrobial peptide LL-37 internalized by immature human dendritic cells alters their phenotype*. Scand J Immunol, 2006. **63**(6): p. 410-9.

31. Paulo, C.S., et al., *Differential internalization of amphotericin B--conjugated nanoparticles in human cells and the expression of heat shock protein 70*. Biomaterials, 2013. **34**(21): p. 5281-93.

32. Ezzat, K., et al., *Scavenger receptor-mediated uptake of cell-penetrating peptide nanocomplexes with oligonucleotides*. FASEB J, 2012. **26**(3): p. 1172-80.

33. Tang, X., et al., *P2X7 Receptor Regulates Internalization of Antimicrobial Peptide LL-37 by Human Macrophages That Promotes Intracellular Pathogen Clearance*. J Immunol, 2015. **195**(3): p. 1191-201.

34. Tokumaru, S., et al., *Induction of keratinocyte migration via transactivation of the epidermal growth factor receptor by the antimicrobial peptide LL-37*. J Immunol, 2005. **175**(7): p. 4662-8.

35. Blobel, C.P., *ADAMs: key components in EGFR signalling and development*. Nat Rev Mol Cell Biol, 2005. **6**(1): p. 32-43.

36. Maretzky, T., et al., *Migration of growth factor-stimulated epithelial and endothelial cells depends on EGFR transactivation by ADAM17*. Nat Commun, 2011. **2**: p. 229.

37. Tomasinsig, L., et al., *The human cathelicidin LL-37 modulates the activities of the P2X7 receptor in a structure-dependent manner*. J Biol Chem, 2008. **283**(45): p. 30471-81.

38. Elssner, A., et al., *A novel P2X7 receptor activator, the human cathelicidin-derived peptide LL37, induces IL-1 beta processing and release*. J Immunol, 2004. **172**(8): p. 4987-94.

39. Mookherjee, N., et al., *Intracellular receptor for human host defense peptide LL-37 in monocytes*. J Immunol, 2009. **183**(4): p. 2688-96.

40. Sperrhacke, M., et al., *SPINK9 stimulates metalloprotease/EGFR-dependent keratinocyte migration via purinergic receptor activation*. J Invest Dermatol, 2014. **134**(6): p. 1645-54.

41. Sommer, A., et al., *Melittin modulates keratinocyte function through P2 receptor-dependent ADAM activation*. J Biol Chem, 2012. **287**(28): p. 23678-89.

42. Volonte, C., et al., *P2X7 receptors: channels, pores and more*. CNS Neurol Disord Drug Targets, 2012. **11**(6): p. 705-21.

43. Honore, P., et al., *A-740003 [N-(1-{[(cyanoimino)(5-quinolinylamino) methyl]amino}-2,2-dimethylpropyl)-2-(3,4-dimethoxyphenyl)acetamide], a novel and selective P2X7 receptor antagonist, dose-dependently reduces neuropathic pain in the rat*. J Pharmacol Exp Ther, 2006. **319**(3): p. 1376-85.

44. Repertinger, S.K., et al., *EGFR enhances early healing after cutaneous incisional wounding*. J Invest Dermatol, 2004. **123**(5): p. 982-9.

45. Lin, Z.Q., et al., *Essential involvement of IL-6 in the skin wound-healing process as evidenced by delayed wound healing in IL-6-deficient mice*. J Leukoc Biol, 2003. **73**(6): p. 713-21.

46. Steinstraesser, L., et al., *Skin electroporation of a plasmid encoding hCAP-18/LL-37 host defense peptide promotes wound healing*. Mol Ther, 2014. **22**(4): p. 734-42.

47. Sehgal, P.B., *Interleukin-6: molecular pathophysiology*. J Invest Dermatol, 1990. **94**(6 Suppl): p. 2S-6S.

48. Niyonsaba, F., et al., *Antimicrobial peptides human beta-defensins stimulate epidermal keratinocyte migration, proliferation and production of proinflammatory cytokines and chemokines*. J Invest Dermatol, 2007. **127**(3): p. 594-604.

49. Hasmann, A., et al., *Analysis of myeloperoxidase activity in wound fluids as a marker of infection*. Ann Clin Biochem, 2013. **50**(Pt 3): p. 245-54.

50. Fernandes, R., et al., *Interactions of skin with gold nanoparticles of different surface charge, shape, and functionality*. Small, 2015. **11**(6): p. 713-21.

51. Randeria, P.S., et al., *siRNA-based spherical nucleic acids reverse impaired wound healing in diabetic mice by ganglioside GM3 synthase knockdown*. Proc Natl Acad Sci U S A, 2015. **112**(18): p. 5573-8.

52. Kalashnikova, I., S. Das, and S. Seal, *Nanomaterials for wound healing: scope and advancement*. Nanomedicine (Lond), 2015. **10**(16): p. 2593-612.

53. Robson, M.C., *Wound infection. A failure of wound healing caused by an imbalance of bacteria*. Surg Clin North Am, 1997. **77**(3): p. 637-50.

54. Conway, A., et al., *Multivalent ligands control stem cell behaviour in vitro and in vivo*. Nat Nanotechnol, 2013. **8**(11): p. 831-8.

55. Miller, C.M., et al., *The role of the P2X(7) receptor in infectious diseases*. PLoS Pathog, 2011. **7**(11): p. e1002212.

56. Tomas, A., C.E. Futter, and E.R. Eden, *EGF receptor trafficking: consequences for signaling and cancer*. Trends Cell Biol, 2014. **24**(1): p. 26-34.

57. Offterdinger, M. and P.I. Bastiaens, *Prolonged EGFR signaling by ERBB2-mediated sequestration at the plasma membrane*. Traffic, 2008. **9**(1): p. 147-55.

58. Hong, S.Y., et al., *CTEN prolongs signaling by EGFR through reducing its ligand-induced degradation*. Cancer Res, 2013. **73**(16): p. 5266-76.

59. Fan, V.H., et al., *Tethered epidermal growth factor provides a survival advantage to mesenchymal stem cells*. Stem Cells, 2007. **25**(5): p. 1241-51.

60. Kahlenberg, J.M. and M.J. Kaplan, *Little peptide, big effects: the role of LL-37 in inflammation and autoimmune disease*. J Immunol, 2013. **191**(10): p. 4895-901.

61. Yu, J., et al., *Host defense peptide LL-37, in synergy with inflammatory mediator IL-1beta, augments immune responses by multiple pathways*. J Immunol, 2007. **179**(11): p. 7684-91.

62. Zheng, D., et al., *Topical delivery of siRNA-based spherical nucleic acid nanoparticle conjugates for gene regulation*. Proc Natl Acad Sci U S A, 2012. **109**(30): p. 11975-80.

Graphical abstract